RSC Advances

PAPER

View Article Online
View Journal | View Issue

Open Access Article. Published on 05 July 2017. Downloaded on 10/20/2025 2:07:39 AM.
This article is licensed under a Creative Commons Attribution-NonCommercial 3.0 Unported Licence.

Check for updates

Cite this: *RSC Adv.*, 2017, 7, 33843

Facile fabrication of hierarchical porous carbon based on extract separated from coal with outstanding electrochemical performance

Peng Chang[a] and Zhihong Qin *[ab]

Received 14th May 2017
Accepted 26th June 2017

DOI: 10.1039/c7ra05437h

rsc.li/rsc-advances

Due to the abundant accessible pores for ion storage, hierarchical short diffusion paths for ion transport, and high diffusion efficiency through macropores, newly developed hierarchical porous carbons (HPCs) have been attracting much attention as one of the most promising electrode materials for high-performance supercapacitors. However, the large-scale production and practical applications of HPCs are still big challenges. Herein, a novel kind of HPCs were directly synthesized from low-cost extracts of coal by coupling nano MgO template with *in situ* KOH activation strategy. During the formation of HPCs, nano-MgO not only serves as structure-directing agent to obtain nanosheet structure, but also plays a critical role in determining the porous system and rate performance of HPCs. The HPCs feature interconnected layered structure with developed hierarchical pore system, and have a high specific surface area up to 3347 m^2 g^{-1}. As electrodes for supercapacitors, the HPCs show a high capacitance of 346 F g^{-1} at 0.5 A g^{-1} in 6 M KOH, an excellent rate performance with capacitance remaining at 262 F g^{-1} at 10 A g^{-1} and a superior cycle stability with 92% capacitance retention after 5000 cycles at 5 A g^{-1}. The fine capacitive performances of HPCs are ascribed to hierarchical pore system, short paths for ion fast transport and 2D layered graphene sheets, make it a promising electrode candidate for high performance supercapacitors.

1. Introduction

Due to the increasingly limited availability of fossil fuel resources, the sustainable energy storage devices that can effectively store and release the electrical energy have drawn considerable attention with the increased demand for the efficient utilization of clean energy resources. Meanwhile, supercapacitors have been recognized as a novel kind of promising energy storage devices in recent years in view of their attractive characteristics such as superior rate capability, high power density, and long cycle life.[1,2]

Generally, the electrochemical properties of supercapacitors largely depend on the electrode materials.[3,4] Various kinds of carbon materials have been adopted as electrode materials for supercapacitors, such as hierarchical porous carbons (HPCs), graphene, carbon nanotubes, carbon fibers, and mesoporous carbons.[5–9] Among those electrochemical active materials, HPCs have been considered as a promising electrode candidate for supercapacitors and deeply investigated owing to their large surface area, electrochemical stability, high conductivity, and low cost.[10]

It is widely known that the existence of micropores is directly responsible for the charge storage to obtain a high specific capacitance while the reasonable meso-/macropores could serve as electrolyte reservoirs and favorable paths which is helpful for fast ion transportation.[11–14] The synergetic effect of unique micro-/meso/macro hierarchical pore system could impart HPCs with superior capacitive property and rate capability in supercapacitor applications.[15] Therefore, the HPCs have been attracting much attention as one of the most promising electrode materials for high-performance supercapacitors due to their huge advantage in unique porosity and it is necessary to develop an efficient method for production of HPCs with ideal porous structure.

Coal as the most affordable energy resource currently being consumed worldwide, is cheap and abundant, and also has been commonly used as carbon source. Up to now, template techniques have been widely employed to synthesize HPCs with well-defined pore characteristics.[16,17] However, the intrinsic mineral matters in raw coal can also serve as the template and cause the collapse of expectant porous structure during the process of acid washing.[18] In a general way, high ash coal was treated with aqua regia, cationic surfactant or NH_4OH to remove the ash content.[19] Nevertheless, these procedures are complicated, time-consuming and high cost. Thus, we introduce a creative extraction and back-extraction method to obtain the desired ash-free group component—loose medium

[a]*School of Chemical Engineering and Technology, China University of Mining & Technology, Xuzhou 221116, P. R. China*
[b]*Key Laboratory of Coal Processing and Efficient Utilization (Ministry of Education), Xuzhou 221116, P. R. China. E-mail: qinzh1210@163.com*

Open Access Article. Published on 05 July 2017. Downloaded on 10/20/2025 2:07:39 AM. This article is licensed under a Creative Commons Attribution-NonCommercial 3.0 Unported Licence.

component (LMC) from raw coal and adopt it as the carbonaceous precursor for synthesis of HPCs.[20,21] What's more, the LMC primarily consists of abundant aliphatic hydrocarbons and aromatic hydrocarbons. During the pyrolysis process, aromatic hydrocarbon molecules featuring sp^2-hybridized carbon atoms could polymerize and aromatize into large interconnected thin layered nano-structure like graphene due to the nanospace confinement of layered template.

Herein, we report a nano layered MgO template strategy coupled with *in situ* KOH activation to synthesize HPCs from LMC which was separated from raw coal. The electrochemical properties of the electrodes prepared from HPCs for supercapacitors were investigated. MgO template plays a critical role in determining the porous structure and electrochemical performance of HPCs and the morphological character could be effectively adjusted *via* the changing of template proportion.

2. Experimental

2.1. Preparation of loose medium component

All chemicals in this experiment were purchased from Aladdin without further purification. Tongting Huaibei raw coal in China was pulverized to pass through a 200 mesh sieve for use. First, 200 g pre-treated coal sample and a mixed extraction agent of 10 L *N*-methyl-2-pyrrolidone (NMP) and 10 L CS_2 were added into extraction kettle and stirred for 3 h. After the extraction process, 20 L deionized water used as back extractant was added into extraction kettle and stirred for 40 min. Then, the back-extraction liquor was layered after standing for 3 h. The lower dark layer was CS_2 layer while the upper layer was water and NMP layer. At last, LMC was obtained by centrifugation of upper layer liquor at a speed of 6000 rpm for 20 min and the yield was about 17%. The proximate and ultimate analyses of raw coal and LMC are listed in Table 1 and the TEM images, infra-red spectrum, and thermogravimetric analysis of LMC have been published in our previous works.[20,21]

2.2. Preparation of HPCs

In a typical run, LMC, nano MgO and KOH were ground respectively, and mixed in mortar with a mass ratio of 1/1/6. The resultant mixture was then activated at 750 °C for 1 hour under nitrogen stream in a tube furnace and the temperature was controllably ramped at a heating rate of 5 °C min^{-1}. The HPC-1 was obtained by washing with 1 M HCl and deionized water repeatedly to remove the template and reaction products. The resulting products were termed as HPC-*X* respectively, where *X* is the ratio of MgO/LMC. For comparison, several ratios of MgO/LMC were evaluated: 0, 1, 3, 5, and 6 with other conditions remaining unchanged. In addition, HPC-0K, HPC-3K samples with the LMC/MgO/KOH mass ratio of 1/5/0, 1/5/3, respectively were also prepared under the same conditions to explore the effect of KOH dosage on the porous structure.

Table 1 Proximate and ultimate analyses of raw coal and LMC

	Proximate analysis (wt%)				Ultimate analysis (wt%)				
Sample	M_{ad}	A_d	V_{daf}	FC_{daf}	C_{daf}	H_{daf}	O_{daf}[a]	N_{daf}	$S_{t,daf}$
Raw coal	1.27	24.20	24.94	75.06	86.50	5.05	6.32	1.47	0.66
LMC	0.48	2.21	27.53	75.63	84.72	5.20	6.72	2.59	0.77

[a] By difference; M_{ad}: moisture (air dried base); daf: dry and ash-free base; A_d: ash (dry base); V_{daf}: volatile matter (dry and ash-free base); $S_{t,daf}$: total sulfur (dry and ash-free base).

2.3. Characterization of HPCs

The porous properties of HPCs were characterized by N_2 adsorption/desorption isotherms at 77 K with an Autosorb-1-MP analyzer (Quantachrome, USA). The specific surface area (S_{BET}) was determined according to the BET (Brunauer–Emmett–Teller) method and the pore size distribution was evaluated by the density functional theory (DFT) method in the calculation model of N_2 at 77 K on carbon (slit pore, NLDFT equilibrium model) from the desorption branches of the isotherms. The total pore volume (V_t) was estimated from the single point adsorption at $P/P_0 = 0.995$. The micropore volume (V_{mic}) was reckoned by the calculation from the HK (Horvath-Kawazoe) model, whereas the non-V_{mic} was calculated from the difference of V_t and V_{mic}. The average pore size (D_{ap}) was identified by the equation of $D_{ap} = 4V_t/S_{BET}$. The microstructures of HPCs and MgO were analyzed by transmission electron microscopy (TEM, FEI Tecnai G^2 F20, USA) and scanning electron microscopy (SEM, FEI Quanta TM 250, USA). The Raman spectra of HPCs were measured on a Raman spectroscopy (Bruker Senterra, Germany) with an excitation wavelength at 532 nm.

2.4. Preparation and electrochemical test of HPCs electrodes

The electrode materials were prepared by mixing 85 wt% of HPCs, 10 wt% of acetylene black, and 5 wt% of polytetrafluoroethylene (PTFE), and then pressed into a thin disk at 5 MPa. The resultant carbon thin disk was pressed onto nickel foam at 5 MPa for 5 min to make supercapacitor electrode. The electrochemical properties of HPCs were investigated using two-electrode cell, while all the electrochemical tests were operated at room temperature using an electrochemical workstation (Ivium Vertex, Holland). The electrolyte was a 6 M KOH aqueous solution and before the electrochemical tests, the electrodes were soaked in electrolyte for 12 h. The button-type supercapacitor was assembled with two electrodes with the similar mass (about 3.6 mg cm^{-2}) separated by a polypropylene membrane. The cyclic voltammetry (CV) curves were recorded over a range of 0–1 V at the sweep rate from 1 to 100 mV and galvanostatic charge–discharge (GCD) measurements were performed at various current densities ranged from 0.5 to 10 A g^{-1} with a potential window of 0–1 V. Electrochemical impedance spectroscopy (EIS) measurements were conducted with an amplitude of 5 mV over a frequency of 100 kHz to 0.001 Hz. The gravimetric capacitance of the HPCs electrode, C (F g^{-1}), could be calculated from the galvanostatic discharge process according to the following equation: $C = 2I\Delta t/m\Delta V$, where I is the discharge current (A), ΔV is the usable voltage after the *IR* drop (V), Δt is the discharge time (s), and m is the mass of active material (g). In addition, the energy density (E, W h kg^{-1}) and

Open Access Article. Published on 05 July 2017. Downloaded on 10/20/2025 2:07:39 AM.
This article is licensed under a Creative Commons Attribution-NonCommercial 3.0 Unported Licence.

power density (P, W kg^{-1}) of the supercapacitors were determined by the following equations: $E = C\Delta V^2/(2 \times 3.6)$, $P = 3600E/\Delta t$, respectively.

3. Results and discussion

3.1. Physical characterizations of HPCs

Fig. 1a–d show the SEM images of the prepared HPCs. It is interesting that under the same magnification, the HPCs possess completely different morphologies with the different dosage of nano MgO template. As displayed in Fig. 1a, HPC-1 shows a rough block pattern with some irregular large holes of a few microns on the outside surface which may be induced by the effusion of pyrolysis gas. In Fig. 1b, HPC-3 presents an unordered sponge-like foam structure and the pore size is mostly in the range of 100–300 nm. While the morphology of HPC-5 manifests a typical layered stacking structure with many small nanosheets and macropores, as provided in Fig. 1c. In the case of HPC-6, the sheet-like structure becomes more integral and homogeneous due to the strict space limitation effect led by excessive template addition. In addition, as marked in each figure, there are a large number of macropores with diameter around 200 nm in HPCs which are inherited from MgO particles. Because the grinding can hardly meet the requirement of mixing uniformly, many macropores could be formed by the remove of stacked and overlapped nano template *via* acid washing. In addition, these macropores can also function as ion-buffering reservoirs to shorten the ion transport distance. Meanwhile, this common feature can not only directly and naturally manifest the developed porous structure of HPCs, especially the part of macropores but also embody hierarchical pore system combined with following pore size distribution analysis. Besides, obviously, the morphology of HPCs can be efficiently adjusted by changing the template dosage. Along with the increase of MgO addition, unordered sponge-like foam structure gradually turns into regular lamellar structure indicating that nano MgO also plays a role of structure-directing during the preparation of HPCs.

Fig. 1e is the TEM image of nano-MgO, in which many sheet-like MgO particles with the size of about 30 nm can be clearly seen. While the TEM observation of HPC-5 (Fig. 1f) reveals a thin and rough layer with abundant ordered micro- and slit mesopores which may be caused by the interlocking of small thin layers or the MgO template embedded vertically on LMC. The big aspect ratio and ideal ratio of micro/mesopores are favorable for ion adsorption and allow fast ion transport across the electrodes which always results in high specific capacitance by forming ion transport expressways. Furthermore, the thin graphene-like sheets are expected to improve the rate performance due to the shortened transport distance of ions.

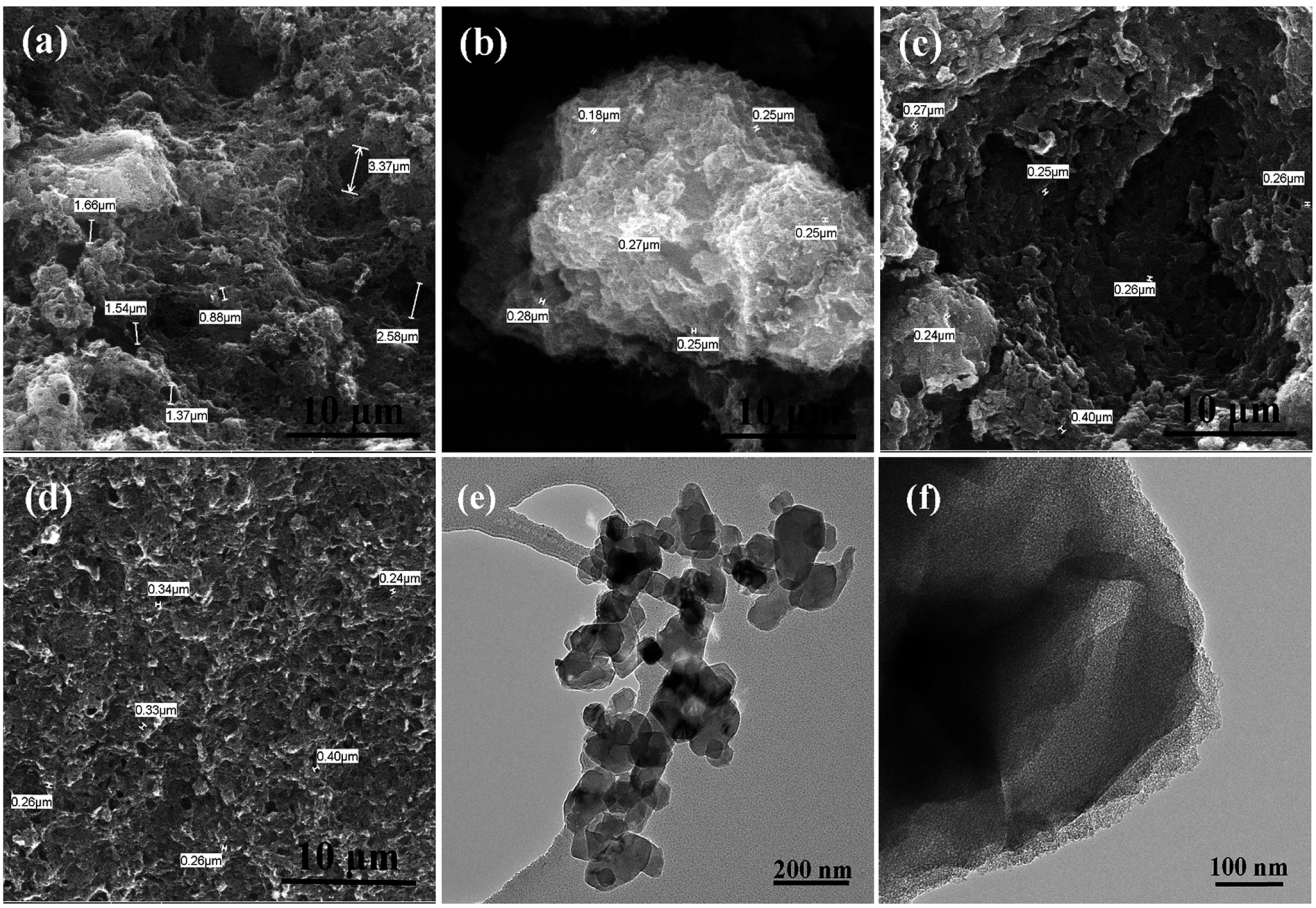

Fig. 1 SEM images of (a) HPC-1, (b) HPC-3, (c) HPC-5, (d) HPC-6; TEM images of (e) nano MgO and (f) HPC-5.

Open Access Article. Published on 05 July 2017. Downloaded on 10/20/2025 2:07:39 AM.
This article is licensed under a Creative Commons Attribution-NonCommercial 3.0 Unported Licence.

For comparison, the pure porous carbon (HPC-0) without nano MgO was also be fabricated, indicative of honeycomb-like structure with many large holes induced by the effusion of pyrolysis gas (Fig. 2a). The HPC-0K under identical conditions in the absence of KOH was also prepared, in which the relatively thick and stacked sheet-like structure can be clearly observed in Fig. 2b. While, the HPC-3K shows a similar morphology with HPC-5. This also implies the structure-directing effect of nano-MgO during the formation of the HPCs and further confirms the space confinement function of template to create a large number of macropores on HPCs.

Based on the SEM and TEM images in Fig. 1 and 2, we can conceive the schematic of the preparation process of HPCs from LMC, as shown in Fig. 3. Firstly, the mixture of LMC and KOH particles was uniformly dispersed on the layered MgO templates. During the annealing process, LMC with high content of aromatic hydrocarbon became soften and melted, and the aromatic hydrocarbon molecules were hold together by the polymerization reactions of active free radicals, and then folded the layered MgO leading to the interconnected thin layered structure of HPCs. In the meantime, the developed hierarchical pore system was created due to the *in situ* activation of the embedded KOH on the formed nano carbon layers and the space confinement effect of MgO template. Finally, the HPCs were obtained after removing the template *via* acid washing.

The detailed porous properties of HPCs were characterized by nitrogen sorption technique. The N_2 adsorption/desorption isotherms and pore size distributions calculated by the DFT method are shown in Fig. 4 and summarized in Table 2. For HPC-0, HPC-1 samples, the adsorption–desorption isotherms exhibit typical characteristics of highly microporous carbon materials, owing to the steep increase of nitrogen adsorption at relative pressure (P/P_0) less than 0.1 which implies the well-developed microporosity and the absence of hysteresis loop at higher P/P_0. As for HPC-3, HPC-5, HPC-6, and HPC-3K, the isotherms reveal combined characteristics of type I and type IV with a H4 type hysteresis loop. It is worth noting that except for the distinct increase in N_2 uptake occurs at P/P_0 less than 0.1, the obvious hysteresis loop at $0.4 < P/P_0 < 0.7$ assigns to the capillary condensation in small-sized mesopores (smaller than 5 nm), suggesting the existence of abundant micropores and mesopores. However, it can also be found that HPC-0K possesses a very underdeveloped microporous structure due to the absence of KOH which can effectively create abundant micropores and high surface area *via* the reaction with carbon matrix: $6KOH + 2C \rightarrow 2K + 3H_2 + 2K_2CO_3$. Besides, compared with the HPC-0, the sharp rise of the N_2 isotherms for HPC-3, HPC-5, HPC-6, HPC-0K, and HPC-3K at a relatively high P/P_0 from 0.9 to 1.0 indicates a great deal of large mesopores and macropores inherited from MgO particles which could facilitate rapider ion mobility and higher charge–discharge rate.[22] These results are also supported by above SEM images.

From Fig. 4b, we can see that all samples present multimodal distribution centered at 1.2, 1.5, 1.7, 2.5, and 4 nm. By comparing the pore size distributions of HPC-0K, HPC-3K, and HPC-5, it can be concluded that these abundant micro- and small mesopores are generated from the KOH activation. The micropores and mesopores of HPC-0, HPC-1 are much less than HPC-3, HPC-5, and HPC-6. There are more mesopores in HPC-5 in comparison to HPC-3 and HPC-6, while in the field of micropores, HPC-3, HPC-5, and HPC-6 have the similar distribution characteristics. This illustrates that the addition of nano MgO promotes the formation of micropores and small mesopores because the thin layered structure induced by the structure-directing effect of MgO template is conducive to the KOH etching reaction, evidenced by the TEM images in Fig. 1. But superfluous template addition may hinder the contact and reaction between KOH and LMC, like HPC-6.

As shown in Table 2, along with the increase of MgO addition, S_{BET} and V_{mic} both gradually increase because the layered structure led by the structure-directing effect of MgO template could contribute to the homogeneous dispersion and reaction of KOH and avoid the over-reaction. As we all know, the *in situ* KOH activation to the thin carbon sheets is much easier than the activation of KOH to the cluster of carbon particles. In addition, as for HPC-6, the undue MgO dosage lowers the relative content of activation agent which eventually causes the drops of S_{BET} and V_{mic}. The HPC-5 possesses the highest specific surface area of 3347 $m^2\ g^{-1}$, the $V_{mic}/V_{non\text{-}mic}$ value of 2.9, indicating a high extent of reactions and an ideal ratio of micro/mesopores which could generate promising electrochemical performance. Meanwhile, for HPC-0, HPC-3K, and HPC-5, the S_{BET} increases from 641 to 3347 $m^2\ g^{-1}$ while the KOH/LMC mass ratio increases from 0 to 6 with other conditions remaining unchanged, demonstrating the positive effect of *in situ* KOH activation on the creation of high surface area and developed pore system.

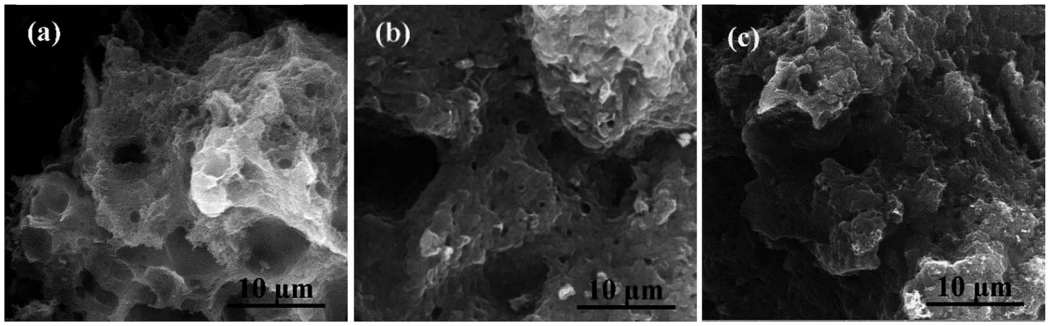

Fig. 2 SEM images of (a) HPC-0; (b) HPC-0K; (c) HPC-3K.

Open Access Article. Published on 05 July 2017. Downloaded on 10/20/2025 2:07:39 AM.
This article is licensed under a Creative Commons Attribution-NonCommercial 3.0 Unported Licence.

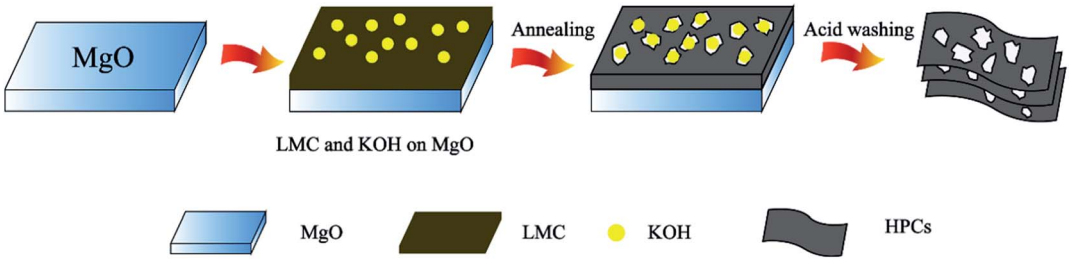

Fig. 3 Schematic of direct preparation process of HPCs from LMC.

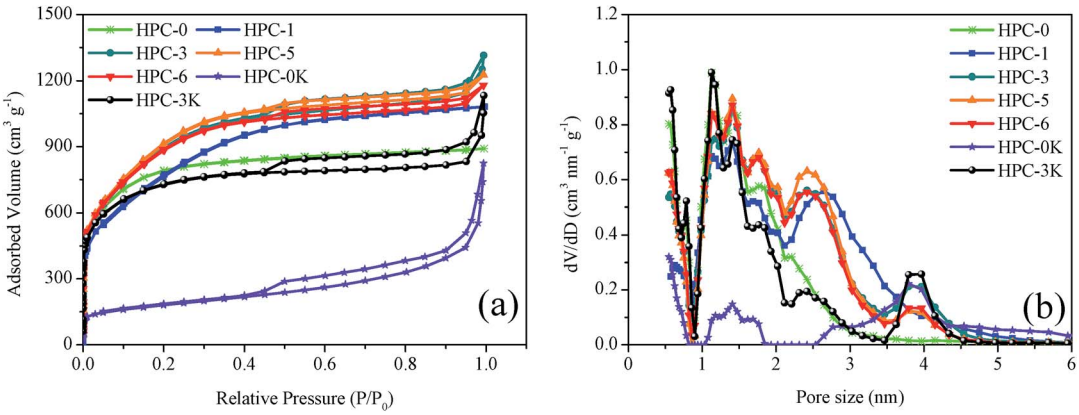

Fig. 4 (a) Nitrogen adsorption/desorption isotherms; (b) pore size distribution of HPCs.

Raman spectroscopy was applied to further analyse the graphitic character of the as-prepared HPCs. As shown in Fig. 5, Raman spectra of HPCs present two apparent Raman-active bands at 1330 cm^{-1} (D-band) associated with a double-resonance effect of amorphous carbonaceous structure, and 1590 cm^{-1} (G-band) which corresponds to the graphite sp^2-bonded carbon atoms in-plane vibrations with E_{2g} symmetry, reflecting the disordered and ideal graphitic lattice respectively.[23–25] A rise in the number of partial lattice defects owing to abundant pores would bring about an increase in the intensity of the D-band and a concomitant drop in the intensity of the G-band. In this paper, the HPCs possess similar porous structure, thus, the peak intensity ratio (I_D/I_G) could be used as an indication of the degree of graphitic structural order.[21] The I_D/I_G of HPC-5 is only 0.83, indicative of a high graphitization degree which is expected to improve the electrochemical behaviors. This result is in well accordance with the TEM observation and N_2 absorption results.

Fig. 6a is the CV curves of all samples at 10 mV s^{-1}. The good quasi-rectangular shapes without obvious redox peaks for all HPCs signify the predominant charge storage mechanism in HPCs to be electric double-layer capacitive behavior. It can also be found that both of the MgO dosage and KOH addition can lead to the enhancement of integral area and a better quasi-rectangular shape which mean the larger capacitance. And the effect of KOH addition is even more visible because the existence of micropores is directly responsible for the charge storage to obtain a high specific capacitance. Meanwhile, the CV curve of HPC-5 exhibits the largest current response and integral area among HPC samples, suggesting the highest capacitance at a relatively low scan rate. Fig. 6b shows the CV curves of HPC-5 at different scan rates. HPC-5 exhibits sustained capacitive behaviors with plateau regions for CV curves at low scan rates, proving the efficient formation of perfect electrical double layers due to the reversible adsorption and desorption of the electrolyte ions in the micropores. It can also be observed that,

Table 2 The porosity parameters of HPCs

Sample	S_{BET} (m^2 g^{-1})	V_{total} (cm^3 g^{-1})	V_{mic} (cm^3 g^{-1})	$V_{non\text{-}mic}$ (cm^3 g^{-1})	D_{ap} (nm)
HPC-0	2574	1.241	1.037	0.204	1.893
HPC-1	2790	1.674	1.101	0.573	2.399
HPC-3	3261	1.774	1.274	0.500	2.175
HPC-5	3347	1.773	1.321	0.452	2.118
HPC-6	3223	1.694	1.269	0.425	2.102
HPC-0K	641	0.857	0.265	0.592	5.348
HPC-3K	2659	1.473	1.085	0.388	2.215

Open Access Article. Published on 05 July 2017. Downloaded on 10/20/2025 2:07:39 AM.
This article is licensed under a Creative Commons Attribution-NonCommercial 3.0 Unported Licence.

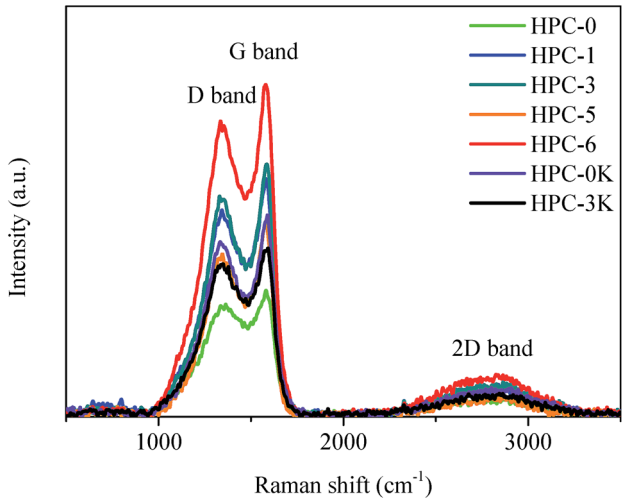

Fig. 5 Raman spectra of HPCs.

at a high scan rate, the mismatch between the diffusion rate of electrolytes and charge transfer speed directly leads to the slight deviation from rectangular shape that implies the relatively poor accessibility of electrolyte ions into electrode surface and finally results in the reduction of charging efficiency and a lessened capacitance.

The capacitance values of HPCs at increasing current loads (from 0.5 to 10 A g^{-1}) were calculated from GCD curves and plotted in Fig. 6c. It can be observed that the discharge capacity goes through a remarkable decay with the increase of current density because of the limited diffusion on the electrode surface.[26] The fading rate of HPC-5 possesses the slowest pace of which the specific capacitance reaches 346 F g^{-1} at 0.5 A g^{-1} and retains 262 F g^{-1} at 10 A g^{-1} with a capacitance retention of 76%, showing the highest capacitance and best rate performance, which may be due to structure merits of developed hierarchical pore system and short paths for ion fast transport on 2D thin graphene-like carbon sheets. Besides, compared with other HPC-*X*, we can find that MgO template plays an active role on the rate performance of electrodes, especially at high current density, owing to the reduced charge transfer resistance which should be ascribed to short paths for ion fast transport provided by the graphene sheets. Moreover, the enhancement of KOH addition can offer more micropores which can directly enhance the specific capacitance of HPCs, as proved by the contrasts among HPC-0K, HPC-3K, and HPC-5.

Fig. 6d presents the Ragone plots of HPCs in 6 M KOH aqueous electrolyte, calculated from the charge–discharge data. It can be found that the energy densities of HPCs drop with the rise of average power densities, which means that less energy can be released at higher rate. As the power density noticeably increases from 921 to 3155 W kg^{-1} at the current density interval of 0.5 to 5 A g^{-1}, the energy density of HPC-5 slowly reduces from 39 to 16 W h kg^{-1}. These results confirm that synergetic effect of developed micro-/meso/macro hierarchical pore system and unique interconnected layered structure can be effectively utilized for charge storage and hint that the as-prepared HPC-5 has the satisfying prospects in the electrochemical devices.

The enhanced kinetics for ion transport and charge transfer in HPCs can be directly proved by Nyquist plots, as illustrated in

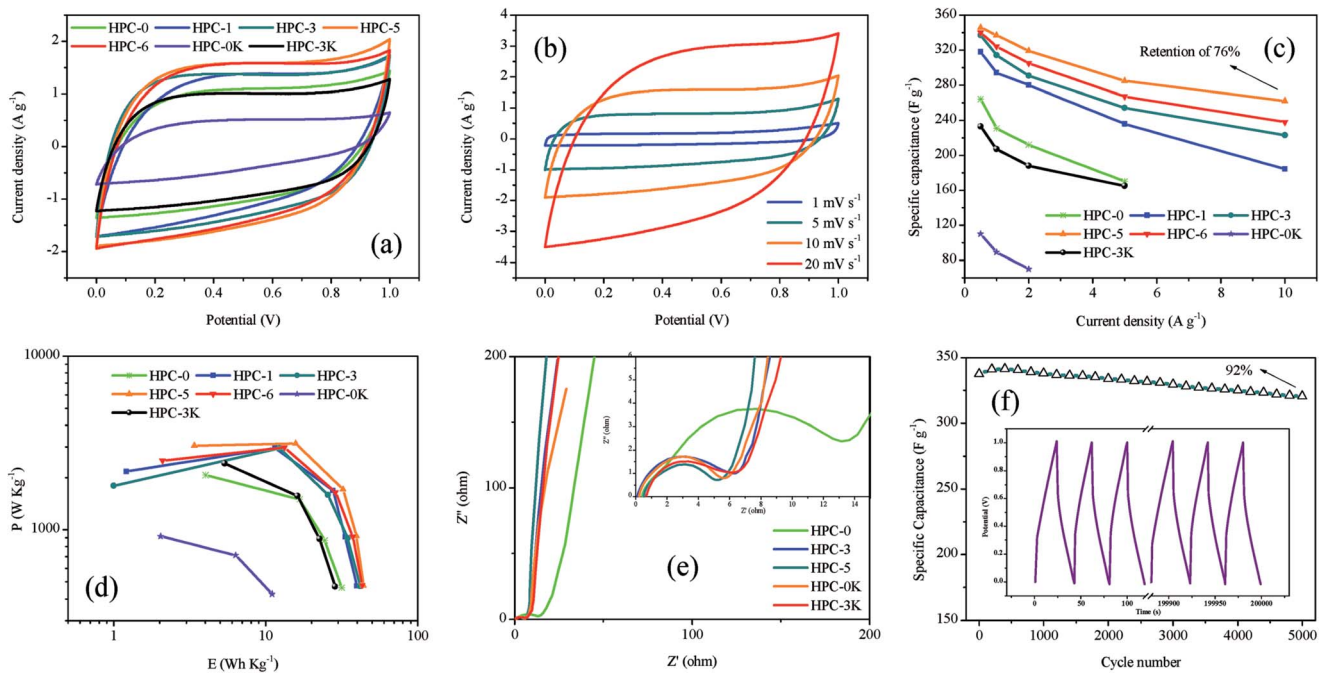

Fig. 6 (a) CV curves of HPCs at 10 mV s^{-1}; (b) CV curves of HPC-5 at different scan rates; (c) specific capacitance of HPCs at different current densities; (d) Ragone plots of HPCs; (e) Nyquist plots of HPCs; (f) cycle stability of HPC-5 measured at 5 A g^{-1} (inset shows the initial and last 3 cycles of charge–discharge curves).

Open Access Article. Published on 05 July 2017. Downloaded on 10/20/2025 2:07:39 AM.
This article is licensed under a Creative Commons Attribution-NonCommercial 3.0 Unported Licence.

Fig. 6e. The diameter of semicircle curve in high frequency area gradually decreases with the increase of nano MgO dosage, demonstrating the lower charge transfer resistance which should be attributed to short paths for ion fast transport and enhanced electrical contact on graphene sheets. Furthermore, it is noteworthy that along with the increase of KOH addition, the linear trend in low frequency region becomes more ideal as a result of the well-developed microporosity which are directly responsible for the charge storage to form a high specific capacitance. These results are also in accordance with the above mentioned capacitive performance and CV curves. As for HPC-5, the low real axis (x) intercept (0.5 ohm), small diameter of the semicircle, short length of the slope segment, and nearly vertical line along the imaginary axis indicate that HPC-5 possesses low equivalent series resistance, charge transfer resistance, ions diffusion resistance, and good conductivity, excellent pore accessibility for the electrolytes, which usually further lead to high specific capacitance.[27]

Fig. 6f exhibits the long-term cycling stability of HPC-5, showing an excellent capacity retention of about 92% over 5000 charge–discharge cycles at 5 A g^{-1}. As shown in the inset of Fig. 6f, the galvanostatic charge–discharge curves still remain triangular shape without obvious pseudocapacitance behavior after 5000 cycles which is the typical characteristic of ideal supercapacitors. The outstanding cycling stability of HPC-5 should be partly ascribed to the combined effect of ideal hierarchical pore system which functions as active sites and expressways for ion adsorption and fast ion transport, and the interconnected lamellar structure with the advantages of high conductivity and structural stability for HPC-5.

The electrochemical performance of HPCs fabricated in this paper has been further compared with other carbon materials without hierarchical structure reported in literature.[21,28–36] Obviously, the specific capacitance and rate performance of HPC-5 are both superior to most of the reported work, as shown in Fig. 7, indicating the great promising of the synthesized HPCs as electrode materials for high performance supercapacitors.

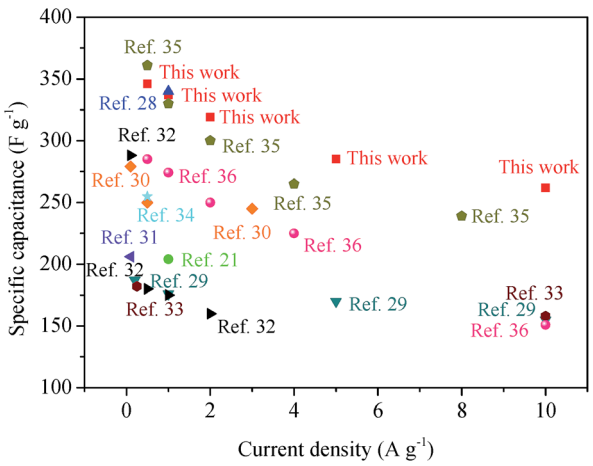

Fig. 7 Comparison of specific capacitance and current density of HPC-5 with other electrodes in aqueous electrolytes.

4. Conclusions

In summary, a novel kind of HPCs has been successfully prepared from the ash-free group component separated from raw coal by extraction and back-extraction method through layered nano MgO template strategy coupled with *in situ* KOH activation. The results show that, during the annealing process, aromatic hydrocarbons in LMC polymerized and transformed into interconnected thin layered structure due to the structure-directing effect of nano-MgO. Meanwhile, the space confinement function of MgO template to create a large number of macropores and the positive effect of *in situ* KOH activation on the formation of high surface area and developed pore system during the preparation of HPCs have both been demonstrated. Specifically, HPC-5 sample exhibits high specific capacitance of 346 F g^{-1} in 6 M KOH aqueous electrolyte, good rate capability of 262 F g^{-1} at 10 A g^{-1} and superior cycling stability with 92% of capacitance retention after 5000 cycles at 5 A g^{-1}. Such excellent electrochemical performance should be assigned to the synergistic effect of unique micro/meso/macro hierarchical pore system, short paths for ion fast transport and 2D layered graphene sheets. Benefited from above great capacitive behaviors and the low cost high ash coal as precursor, the prepared novel hierarchical porous carbon materials present great potential for practical application as an electrode material for supercapacitors.

Acknowledgements

This work has been performed with financial support from National Natural Science Foundation of China (No. 51674260, 51274201).

References

1 P. Simon and Y. Gogotsi, *Nat. Mater.*, 2008, **7**, 845.
2 S. Kondrat, C. R. Pérez, V. Presser, Y. Gogotsi and A. A. Kornyshev, *Energy Environ. Sci.*, 2012, **5**, 6474.
3 M. R. Lukatskaya, O. Mashtalir, C. E. Ren, Y. Dallagnes, P. Rozier, P. L. Taberna, M. Naguib, P. Simon, M. W. Barsoum and Y. Gogosti, *Science*, 2013, **341**, 1502.
4 K. Kotz and M. Carlen, *Electrochim. Acta*, 2000, **45**, 2483.
5 P. Sivaraman, S. P. Mishra, D. D. Potphode, A. P. Thakur, K. Shashidhara, A. B. Samui and A. R. Bhattacharyya, *RSC Adv.*, 2015, **5**, 83546.
6 L. P. Wang, Y. Zhou and J. S. Qiu, *Microporous Mesoporous Mater.*, 2013, **174**, 67.
7 L. L. Zhang and X. S. Zhano, *Chem. Soc. Rev.*, 2009, **38**, 2520.
8 E. Frackowiak and F. Beguin, *Carbon*, 2002, **40**, 1775.
9 J. Y. Qu, F. Gao, Q. Zhou, Z. Y. Wang, H. Hu, B. B. Li, W. B. Wan, X. Z. Wang and J. S. Qiu, *Nanoscale*, 2013, **5**, 2999.
10 X. Y. Zhang, X. Y. Wang, L. L. Jiang, H. Wu, C. Wu and J. C. Su, *J. Power Sources*, 2012, **216**, 290.
11 D. D. Zhou, Y. J. Du, Y. F. Song, Y. G. Wang, C. X. Wang and Y. Y. Xia, *J. Mater. Chem. A*, 2013, **1**, 1192.
12 S. L. Jin, H. G. Deng, L. Zhan, W. M. Qiao and L. C. Ling, *New Res. Carbon Mater.*, 2012, **27**, 87.

Open Access Article. Published on 05 July 2017. Downloaded on 10/20/2025 2:07:39 AM.
This article is licensed under a Creative Commons Attribution-NonCommercial 3.0 Unported Licence.

13 W. Lu, S. Huang, L. Miao, M. Liu, D. Zhu, L. Li, H. Duan, Z. Xu and L. Gan, *Chin. Chem. Lett.*, 2017, **28**, 1324.
14 L. Miao, H. Duan, M. Liu, W. Lu, D. Zhu, T. Chen, L. Li and L. Gan, *Chem. Eng. J.*, 2017, **317**, 651.
15 Y. R. Liang, B. M. Wu, D. C. Wu, F. Xu, Z. H. Li, J. W. Luo, H. Zhong, R. W. Fu and K. Matyjaszewski, *J. Mater. Chem.*, 2011, **21**, 14424.
16 W. F. Zhang, Z. H. Huang, G. P. Cao, F. Y. Kang and Y. S. Yang, *J. Power Sources*, 2012, **204**, 230.
17 Y. Luan, Y. W. Xue and Z. G. Shi, *Mater. Lett.*, 2012, **88**, 30.
18 J. B. Zhang, L. J. Jin, J. Cheng and H. Q. Hu, *Carbon*, 2013, **55**, 221.
19 G. X. Huang, W. W. Kang, B. L. Xing, L. J. Chen and C. X. Zhang, *Fuel Process. Technol.*, 2016, **142**, 1.
20 Z. H. Qin, C. L. Hou, J. Chen, L. Zhang and J. Ma, *Int. J. Min. Sci. Technol.*, 2009, **19**, 636.
21 P. Chang and Z. H. Qin, *Int. J. Electrochem. Sci.*, 2017, **12**, 1846.
22 B. H. Kim and K. S. Yang, *Electrochim. Acta*, 2013, **88**, 597.
23 D. W. Wang, F. Li, M. Liu, G. Q. Lu and H. M. Cheng, *Angew. Chem., Int. Ed.*, 2008, **47**, 373.
24 Y. P. Zhai, Y. Dou, X. X. Liu, S. S. Park, C. S. Ha and D. Zhao, *Carbon*, 2011, **49**, 545.
25 M. Liu, X. Ma, L. Gan, Z. Xu, D. Zhu and L. Chen, *J. Mater. Chem. A*, 2014, **2**, 17107.
26 G. W. Sun, W. H. Song, X. J. Liu, D. H. Long, W. M. Qiao and L. C. Ling, *Electrochim. Acta*, 2011, **56**, 9248.
27 A. Lewandowski, A. Olejniczak, M. Galinski and I. Stepniak, *J. Power Sources*, 2010, **195**, 5814.
28 W. J. Qian, F. X. Sun, Y. H. Xu, L. H. Qiu, C. H. Liu, S. D. Wang and F. Yan, *Energy Environ. Sci.*, 2014, **7**, 379.
29 W. F. Zhang, Z. H. Huang, C. J. Zhou, G. P. Cao, F. Y. Kang and Y. S. Yang, *J. Mater. Chem.*, 2012, **22**, 7158.
30 F. Gao, G. H. Shao, J. Y. Qu, S. Y. Lv, Y. Q. Li and M. B. Wu, *Electrochim. Acta*, 2015, **155**, 201.
31 J. Y. Qu, C. Geng, S. Y. Lv, G. H. Shao, S. Y. Ma and M. B. Wu, *Electrochim. Acta*, 2015, **176**, 982.
32 X. J. He, Y. J. Geng, J. S. Qiu, M. D. Zheng, S. A. Long and X. Y. Zhang, *Carbon*, 2010, **48**, 1662.
33 H. J. Wang, L. Zhi, K. Q. Liu, L. Q. Dang, Z. H. Liu, Z. B. Lei, C. Yu and J. S. Qiu, *Adv. Funct. Mater.*, 2015, **25**, 5420.
34 A. M. Abdelkader, *J. Mater. Chem. A*, 2015, **3**, 8519.
35 M. G. Deng and R. Q. Wang, *New Res. Carbon Mater.*, 2013, **28**, 262.
36 X. Li, W. Xing, S. P. Zhuo, J. Zhou, F. Li, S. Z. Qiao and G. Q. Lu, *Bioresour. Technol.*, 2011, **102**, 1118.

 This journal is © The Royal Society of Chemistry 2017